ACS Catalysis

Research Article

pubs.acs.org/acscatalysis

In Situ Infrared Spectroscopic Investigations of Pyridine-Mediated CO_2 Reduction on Pt Electrocatalysts

Marco Dunwell, Yushan Yan,* and Bingjun Xu*

Center for Catalytic Science and Technology, Department of Chemical and Biomolecular Engineering, University of Delaware, Newark, Delaware 19716, United States

Supporting Information

ABSTRACT: Pyridine-mediated electrochemical reduction of CO_2 has attracted much attention owing to the promise of producing valuable oxygenates with high yields. However, no detectable level of methanol was observed in the pyridine-mediated CO_2 electrolysis on Pt over the entire potential range investigated (−0.2 to −0.8 V vs RHE) in this study. Formate was observed at a potential below −0.6 V vs RHE in the absence and presence of pyridine, but the presence of pyridine does accelerate the rate of formate production. Numerous reaction mechanisms have been proposed on the basis of reactivity measurements, cyclic voltammetry, or computational methods; however, a direct experimental mechanistic investigation has been lacking. By employing surface-enhanced infrared absorption spectroscopy, we identified an adsorbed unidentate $COOH_L$ intermediate on Pt regardless of the presence of pyridine. Surface coverage of the $COOH_L$ intermediate relative to that of adsorbed CO appears to increase with the concentration of pyridine in the electrolyte, which is consistent with the observed production rates for formate and CO. We propose that adsorbed $COOH_L$ is a common intermediate in the formation of both formate and CO, and the presence of pyridinium promotes the formate pathway.

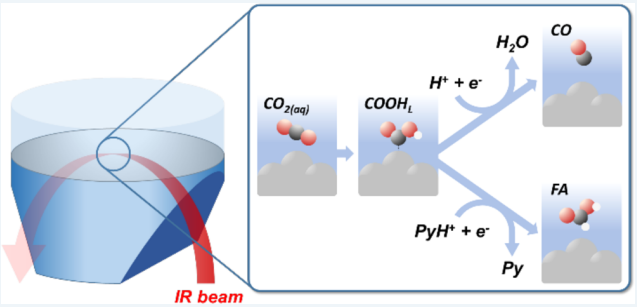

KEYWORDS: *CO_2, electrochemical reduction, pyridine, attenuated total reflectance surface-enhanced infrared absorption spectroscopy, formate, carbon monoxide, mechanism*

INTRODUCTION

Growing concerns about rising atmospheric CO_2 concentrations have led to an increase in research into the electrochemical reduction of CO_2.[1−3] The majority of work up to this point has been studying the CO_2 reduction reaction (CO_2RR) in aqueous bicarbonate solutions.[1,2] Although some monometallic catalysts have shown impressive selectivity toward $2e^-$ transfer products (carbon monoxide and formate), only Cu produces further reduction products such as methanol and ethylene.[1,2] Poor selectivity toward these valuable products, however, has been a major barrier to the advancement of the electrochemical CO_2RR on Cu electrodes. Seeking to improve the selectivity toward these valuable products, in 1994, the Bocarsly group first demonstrated that the addition of 10 mM pyridine (Py) to 0.5 M $NaClO_4$ could help promote the selective formation of methanol on typically hydrogen and carbon monoxide selective Pd electrodes.[4,5] Using a hydrogenated Pd electrode, they showed that methanol could be produced with up to 30% Faradaic efficiency along with a small amount of formaldehyde as a byproduct. It is noted, however, that this high selectivity turned out to be difficult to replicate by others. Portenkirchner et al. reached a maximum Faradaic efficiency of 15%, while Costentin et al. were only able to produce <2% Faradaic efficiency toward methanol under similar experimental conditions.[6,7] It was initially proposed that pyridinium ions (PyH^+) in the electrolyte could be reduced to form a highly active pyridinium radical, which in turn reacted with CO_2 in a series of steps to produce methanol and formate on Pt electrodes.[5,8,9] Computational studies of this system suggested a variety of possible alternative mechanisms.[10−14] Keith et al. proposed that both 4,4′-bipyridine and *p*-dihydropyridine, formed through the reduction of PyH^+, could serve as cocatalysts in the pyridine-mediated CO_2RR (Py-CO_2RR).[10−12] Lim et al. proposed similar mechanisms for photocatalyzed Py-CO_2RR systems.[13,14] Additional computational work in 2013 by Ertem et al. showed that the formation of the PyH^+ radical would not be possible until much lower electrode potentials, calling into question the originally proposed mechanism.[15] Rather, the authors first suggested that the initial formation of formate in the Py-CO_2RR proceeded through a proton-coupled hydride transfer following the reduction of PyH^+ to surface-adsorbed hydrogen (H_{ad}) and Py.[15] Subsequent work by the Bocarsly group investigating the cyclic voltammograms (CVs) of other weak acids supported the assignment that the cathodic peak in the CV was due to the reduction of PyH^+ to H_{ad} and Py.[16] In light of these

Received: April 28, 2017
Revised: June 27, 2017
Published: July 5, 2017

DOI: 10.1021/acscatal.7b01392
ACS Catal. 2017, 7, 5410−5419

advancements, Bocarsly and co-workers proposed a new mechanism based on electrokinetic analysis and isotopic labeling.[17,18] PyH^+ is first produced in solution through the equilibrium with Py around pH 5.3. H_{ad} is then formed on the Pt surface through the reduction of either PyH^+ or hydronium, which then reacts with a PyH^+-CO_2 complex to form formic acid and Py. Further reduction to methanol and formaldehyde is proposed to occur in solution with PyH^+ acting as a proton donor in subsequent steps toward the formation of methanol. Despite numerous experimental and computational studies of this system, there is still debate in the literature regarding the reaction mechanism. In particular, spectroscopic evidence that supports or refutes the current proposed pathways is still lacking. In this work, we conducted reactivity studies in order to test the reproducibility of previous work and report the first in situ spectroscopic investigation of the Py-CO_2RR using attenuated total reflectance surface-enhanced infrared absorption spectroscopy (ATR-SEIRAS) to test the viability of previously proposed mechanisms based on both computational and electrochemical studies.

METHODS

In Situ ATR-SEIRAS Experiments. Polycrystalline Pt and Au nanofilms, deposited chemically on the reflecting plane of a Si prism cut to a 60° angle of incidence, served as the working electrodes. Detailed preparation procedures for the SEIRAS active film electrodes have been described in our previous work.[19,20] A two-compartment spectroelectrochemical cell, separated by a cation-exchange membrane (Nafion 1135), was designed to accommodate the Si prism and to avoid/reduce any possible cross-contamination from the counter electrode (Figure S1 in the Supporting Information) or back-oxidation of reduction products. ATR-SEIRAS experiments were conducted on an Agilent Technologies Cary 660 FTIR spectrometer equipped with a liquid-nitrogen-cooled MCT detector and a modified Pike Technologies VeeMAX II ATR accessory. The spectrometer was coupled with a Solartron SI 1260/1287 system for electrochemical measurements. The counter electrode was a Pt mesh for all Pt-film working electrode (WE) experiments and a graphite rod for all Au-film WE experiments. The reference was an Ag/AgCl electrode (3.0 M KCl, BASi). Impedance measurements were conducted at the beginning of each experiment, and the internal resistance (typically 20−30 Ω) was actively corrected for throughout spectroelectrochemical experiments. All spectra were collected with a 4 cm^{-1} resolution. Spectra are presented in absorbance where positive and negative peaks signify an increase and decrease in the corresponding interfacial species, respectively. All potentials are given on the reversible hydrogen electrode (RHE) scale unless noted otherwise.

Electrochemical Reactivity Experiments. A Princeton Applied Research VersaSTAT 3 potentiostat was used for electrochemical reactivity studies. Electrolysis was performed at room temperature in a gastight two-compartment electrochemical cell using a piece of cation exchange membrane (Nafion 1135) as the separator. The working electrode compartment contained 9 mL of electrolyte and 9 mL of headspace. Pt foil (Alfa Aesar, 99.99%) and Pt mesh were used as the working and counter electrodes, respectively, and Ag/AgCl (3.0 M KCl, BASi) was used as the reference electrode. The working and counter electrodes were cleaned via piranha etch (3/1 by volume of H_2SO_4/H_2O_2) prior to each electrolysis. The electrolyte consisted of 0.5 M KCl (Fisher Chemical, >99%) as a supporting electrolyte with 0.0, 0.1, or 0.01 M pyridine (Sigma-Aldrich, 99.8%) added. The pH of the electrolyte was adjusted in each case to 5.3 prior to CO_2 saturation using concentrated H_2SO_4 (Sigma-Aldrich, 99.999%). Before electrolysis the electrolyte was purged with CO_2 (Matheson) for at least 1 h, and the headspace of the electrochemical cell was purged for at least 10 min to saturate the electrolyte with CO_2 and ensure 1 atm of CO_2 in the headspace. During the electrolysis, the working electrode chamber was stirred at a rate of 800 rpm using a magnetic stirrer. Internal resistance was determined before each electrolysis (typically <10 Ω) and corrected for as data were collected. Gas-phase products were collected using a gastight syringe (Hamilton) to assess catalyst selectivity and partial current density of the products. Quantification of gas-phase products was performed using a gas chromatograph (Agilent, 7890B). Liquid-phase products were quantified using an AV 600 II NMR spectrometer with acetonitrile as an internal standard. Briefly, NMR samples were prepared by mixing 0.4 mL of the sample solution with 0.1 mL of 0.05 M acetonitrile internal standard in D_2O.

RESULTS AND DISCUSSION

Reactivity of the Py-CO_2RR. Reactivity studies were conducted to resolve the discrepancies between previous works on the pyridine-mediated CO_2 reduction reaction (Py-CO_2RR). Cyclic voltammograms collected on a Pt foil in 0.01 M pyridine with 0.5 M KCl as the supporting electrolyte (with pH adjusted to 5.3 using H_2SO_4) under both Ar and CO_2 purge are in good agreement with previous experimental work (Figure S2 in the Supporting Information).[8] Peaks due to the reduction of the pyridinium cation (PyH^+) to adsorbed hydrogen (H_{ad}) and pyridine (Py) are observed at −0.1 V. This peak is absent when there is no pyridine in the electrolyte at the same pH, confirming that this feature is related to the reduction of PyH^+, rather than H^+ (Figure S2). An increase in current was observed under CO_2 purge relative to Ar, likely due to the additional CO_2RR current. Initial reactivity studies were conducted under conditions similar to those outlined by Bocarsly et al.[8] (i.e., −50 μA cm^{-2} for 20 h in CO_2-saturated solution of 0.01 M pyridine with 0.5 M KCl as the supporting electrolyte); however, neither methanol nor formate was observed under these experimental conditions. The detection limit of methanol with liquid-phase NMR is determined to be 0.0005 mM (Figure S3 in the Supporting Information). Lack of methanol production in Py-CO_2RR under similar conditions has been reported before.[6] Consequently, additional experiments were performed under potentiostatic electrolysis at −0.2, −0.4, −0.6, and −0.8 V until 16 C of charge had been passed to determine the ideal potential for the Py-CO_2RR (Table S1 in the Supporting Information). Electrolysis at −0.2 and −0.4 V produced neither formate nor methanol within the detection limit of NMR. After 16 C of charge at −0.2 V, the detection limit of 0.0005 mM methanol via NMR corresponds to a Faradaic efficiency (FE) of 0.03%. At −0.6 V formate was produced with an FE of <0.1%. At −0.8 V an FE of ∼2% toward formate was achieved. No detectable amount of methanol was observed in either case, indicating that the rate of the proposed liquid-phase reduction of formate,[17] if it exists, is below our detection limit. It should also be noted that after electrolysis the pH of the electrolyte in both the working and counter electrode had changed, increasing and decreasing by <1 pH unit in the working and counter electrode chambers,

DOI: 10.1021/acscatal.7b01392
ACS Catal. 2017, 7, 5410−5419

Table 1. Faradaic Efficiencies of the Py-CO_2RR[a]

[Py]/M	Nafion	j/mA cm^{-2}	Faradaic efficiency/%			
			CO	formate	H_2	total
0.0	yes	−0.97	0.14 ± 0.12	0.37 ± 0.37	101.1 ± 3.2	101.6 ± 3.7
0.01	yes	−1.59	0.54 ± 0.21	2.37 ± 0.47	84.6 ± 0.9	87.5 ± 1.5
0.1	yes	−7.27	0.01 ± 0.00	0.62 ± 0.04	35.6 ± 1.7	36.5 ± 1.7
0.01	no	−8.11	0.04 ± 0.02	1.00 ± 0.17	22.9 ± 0.1	23.9 ± 0.3
0.1	no	−14.66	0.01 ± 0.00	0.79 ± 0.06	22.9 ± 1.0	23.7 ± 0.9

[a]Electrolysis was conducted for 4 h at −0.8 V with various Py concentrations and 0.5 M KCl as the supporting electrolyte under 1 atm of CO_2 on Pt-foil electrodes. Ranges given are the standard errors estimated using at least three repeats.

Table 2. Production Rates of Various Py-CO_2RR Products[a]

[Py]/M	Nafion	j/mA cm^{-2}	rate/10^{10} mol s^{-1}		
			CO	formate	H_2
0.0	yes	−0.97	0.14 ± 0.12	0.36 ± 0.36	127.7 ± 25.0
0.01	yes	−1.59	0.91 ± 0.39	4.00 ± 0.93	142.0 ± 6.7
0.1	yes	−7.27	0.09 ± 0.00	4.33 ± 0.52	248.5 ± 3.8
0.01	no	−8.11	0.34 ± 0.13	11.1 ± 4.23	243.2 ± 56.0
0.1	no	−14.66	0.16 ± 0.01	11.6 ± 1.12	334.6 ± 8.6

[a]Electrolysis was conducted for 4 h at −0.8 V with various Py concentrations and 0.5 M KCl as the supporting electrolyte under 1 atm of CO_2 on Pt-foil electrodes. Ranges given are the standard errors estimated using at least three repeats.

respectively, in good agreement with previous work.[7] On the basis of the results of these exploratory experiments, all additional reactivity studies were conducted at −0.8 V to maximize the formate production rate and efficiency.

Additional electrolysis using different Py concentrations (Tables 1 and 2) show that 0.01 M Py yields higher CO_2RR selectivity than both the [Py] = 0.0 M and [Py] = 0.1 M cases, although the vast majority of current goes to the hydrogen evolution reaction (HER). In all cases, a small amount of CO and formate were produced, but again, no detectable level of methanol was observed under any conditions tested. From 0.0 to 0.01 M Py, both the overall current and selectivity toward CO and formate increase, suggesting that, although no methanol is produced, the presence of Py does promote the CO_2RR over the HER on Pt electrodes. As [Py] is increased further to 0.1 M, although the total current density continues to increase, selectivity toward formate decreases to a value between those of 0.0 and 0.01 M Py, suggesting that 0.01 M is near the optimal concentration for the promotion of the CO_2RR on Pt when selectivity is considered. The overall rate of formate production increases with increasing [Py] (Table 2). The increase in total current with increasing [Py] can be attributed to an increase in buffer capacity of the electrolyte with increasing [Py]. As the reaction proceeds in the unbuffered electrolyte (0.0 M Py), the pH near the electrode surface increases as the HER proceeds. The increase in surface pH corresponds to a decrease in overpotential for both the CO_2RR and the HER, leading to a decrease in overall current. When [Py] is increased, the buffer capacity of the electrolyte increases as well due to the equilibrium between Py and PyH^+, which combats the changes in surface pH during electrolysis and maintains the correct RHE potential during electrolysis.

It is also important to note that, as the overall current increases, the charge balance becomes increasingly poor, from ∼100% in 0.0 M Py to <40% in 0.1 M Py when the working and counter electrodes are separated by a Nafion membrane. It is unlikely that the poor charge balance is due to products leaking out of the electrochemical cell, as each experiment was repeated at least three times with good agreement between each repeat (Table 1). The unaccounted-for charge as the current density increases is proposed to be due to the formation of reactive intermediate species produced at the anode, e.g., during the oxygen (OER) and chlorine (CER) evolution reactions. As the overall current increases, a growing overpotential is required for the anodic reactions. We propose that higher overpotentials for the OER and/or CER lead to the formation of reactive intermediates, which are then either subsequently reduced at the cathode, leading to a closed current loop without the production of observable products, or react to oxidize other species in the solution, including CO_2RR products, contributing to the observed low selectivity for the CO_2RR. This hypothesis was tested by adding small aliquots of dimethyl sulfoxide (DMSO) to the electrolyte to both the anode and cathode chambers immediately after electrolysis (Figure S4 in the Supporting Information). Upon addition of DMSO to the postelectrolysis solution from the counter electrode, the DMSO reacts with the intermediates produced at the anode to generate dimethylsulfone ($DMSO_2$), as determined using both ^{1}H NMR (Figures S4 and S5a in the Supporting Information) and ^{13}C NMR spectroscopy (Figure S5b). When DMSO was added to the postelectrolysis solution from the cathode, however, there was a decrease of 2 orders of magnitude in DMSO conversion (Figure 4d), suggesting that the reactive species are indeed produced at the anode and that the Nafion separator allows a small fraction of the oxidizing species to cross over to the cathode chamber. It is likely that these reactive oxidants react with CO_2RR intermediates, leading to the low efficiencies observed as well as the lack of methanol. It is important to note that these species do not react directly with methanol, as determined by the lack of methanol conversion after adding it to the postelectrolysis solution.

Additional reactivity studies conducted in 0.01 and 0.1 M Py without the use of the Nafion separator are also consistent with these findings. When the anode and cathode are not separated by the Nafion membrane, the overall current density increases due to the more efficient transport of the reactive intermediates to the cathode where they can be reduced, leading to significant currents with no observable products. This is reflected in the

DOI: 10.1021/acscatal.7b01392
ACS Catal. 2017, 7, 5410−5419

decreased FE in reactivity studies without the separator in place (<25%, Table 1). In 0.01 M Py, FE toward formate decreases from ∼2.4% with a Nafion membrane to ∼1.0% when the anode and cathode are not separated (Table 1).

While the exact nature of the reactive species is still unclear, they are highly energetic and unstable in the electrolyte. Since two-electron oxidation of water to hydrogen peroxide on Pt has been reported as a side reaction of the OER, hydrogen peroxide could be the reactive species produced at the anode. However, no conversion of DMSO to $DMSO_2$ was observed when 0.1 M H_2O_2 was introduced into an aqueous solution of DMSO, suggesting that the reactive species is more oxidizing than H_2O_2. Moreover, when DMSO was introduced to the postelectrolysis solution several hours after the electrolysis, no formation of $DMSO_2$ was detected, indicating that the reactive species slowly decompose in the electrolyte. Studies of DMSO conversion in atmospheric chemistry have shown that DMSO is readily oxidized by both $OH^•$ and $ClO^•$ radicals, with $DMSO_2$ as a major product.[21,22] We propose that OH and Cl (which reacts with O_2 to form $ClO^•$) radical intermediates formed in the OER and CERs are the active oxidant species responsible for the poor charge balance and conversion of DMSO in these experiments. Additional experiments using $KClO_4$ show no conversion of DMSO with electrolyte from either the anode or cathode chamber (Figure S4 in the Supporting Information, purple trace), suggesting that the $ClO^•$ radical is the most likely culprit for the oxidation of DMSO to $DMSO_2$.

Spectroscopic Investigations of the Py-CO_2RR. To gain a more thorough understanding of observed reactivity trends, as well as to help resolve discrepancies in previous mechanistic studies of the Py-CO_2RR, in situ SEIRAS was employed to gain insights into the mechanism of the cathode-mediated reactions. Due to the complexity of the system, we first studied the CO_2RR in a Py-free solution of 0.5 M KCl under CO_2 purge. The potential was stepped from 1.0 to −0.4 V, and spectra were collected in 0.1 V increments using 1.0 V as the reference potential (Figure 1). As the potenial was decreased, two large peaks emerged around 1990 and 1760 cm^{-1}, beginning at 0.2 V and increasing with decreasing potential. The higher wavenumber peak can be attributed to linearly bound CO (CO_L) on Pt. We attribute the lower wavenumber peak to a convolution of both bridge-bound CO (CO_B) and linearly bound, unidentate carboxyl species ($COOH_L$), which will be discussed in more detail shortly. Initial observation of adsorbed CO intermediates above the equilibrium potential for CO_2 reduction to CO can be explained by a shift in the equilibrium potential from the standard equilibrium potential due to the low initial partial pressure of CO according to the Nernst equation.[23] The initial blue shift in the position the CO_L peak with the decreasing electrode potential is due to the increasing coverage of CO, while the red shift of the peak at potentials below 0 V can be attributed to the Stark tuning effect.[24,25] The lower wavenumber band blue-shifts monotonically with decreasing potential, suggesting that its origin is more complex. Observation of intermediates toward the production of both CO and formate is consistent with the reactivity studies, which showed that, even in the absence of Py, a small amount of each species is produced. On the basis of the high coverage of CO at low potentials, it is likely that the rate of CO production in 0.5 M KCl is limited by the irreversible adsorption of CO on Pt, blocking reaction sites for the CO_2RR.

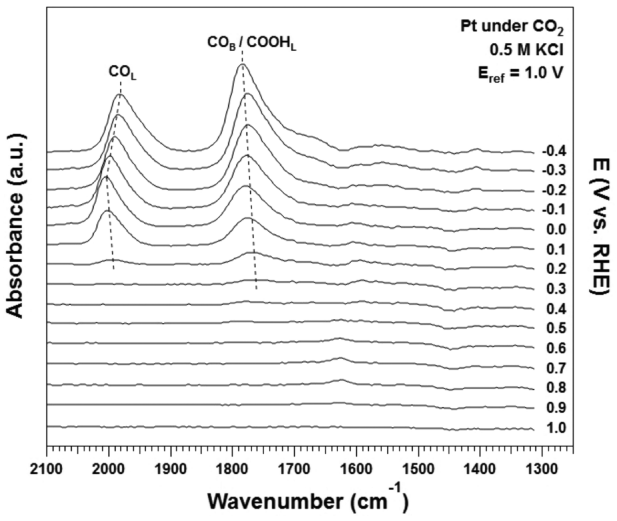

Figure 1. ATR-SEIRA spectra (4 cm^{-1} resolution, 64 coadded scans) during potentiostatic electrolysis from 1.0 to −0.4 V in 0.5 M KCl under 1 atm of CO_2 on Pt-film electrodes. The pH was adjusted to 5.3 prior to CO_2 saturation with H_2SO_4 and did not change upon addition of CO_2. The reference spectrum was collected at 1.0 V.

CO was introduced to Pt in the absence of CO_2 and pyridine and monitored with SEIRAS to understand its adsorption behavior. A solution of 0.01 M Py with 0.5 M KCl was prepared, and the potential was held at −0.4 V under Ar until the spectra equilibrated (Figure 2a). A small, broad peak at 2050 cm^{-1} was observed, which is attributed to adsorbed hydrogen (H_{ad}) from the HER, red-shifted from ∼2090 cm^{-1} as observed in 0.1 M $HClO_4$ due to Stark tuning (Figure S6 in the Supporting Information).[26−28] Once the spectra had reached equilibrium, CO was introduced to the solution while the surface state was monitored by SEIRAS. Both the CO_L and CO_B peaks exhibited monotonic growth as the solution became CO-saturated and the Pt electrode reached its equilibrium coverage. Peak positions after equilibrium coverage had been reached are consistent with previous reports.[19,29,30]

Sequential doses of CO_2 and CO at −0.4 V show that the band at 1761−1784 cm^{-1} shown in Figure 1 corresponds to at least two distinctive species. When the same experiment as in Figure 2a was repeated, except for replacing Ar with CO_2, two bands grew with time initially and then stabilized (Figure 2b). The higher wavenumber band can be unequivocally assigned to CO_L, while the assignment of the lower wavenumber band from 1815 to 1850 cm^{-1} is more involved. It is important to note here that the blue shift of both the higher and lower wavenumber bands in Figure 2 relative to Figure 1 can be explained by an increase in surface coverage of these species. The initial CO_2-saturated spectra in Figure 2 were collected after the spectra had reached a steady state, whereas in Figure 1 spectra were collected shortly after each potential step, so that an equilibrium coverage had not yet been reached. After equilibration of the spectra under the CO_2 atmosphere, the gas purge was switched from CO_2 to CO as the potential was held at −0.4 V. As the surface gradually became CO-saturated, the position of both CO bands gradually shifted to higher wavenumber (Figures 2b and 3a). Interestingly, the intensity of the lower wavenumber band decreased before it grew again as the surface reached equilibrium CO coverage, while the intensity of the CO_L band exhibited monotonic growth (Figure 3b). The nonmonotonic growth of the lower wavenumber band

DOI: 10.1021/acscatal.7b01392
ACS Catal. 2017, 7, 5410−5419

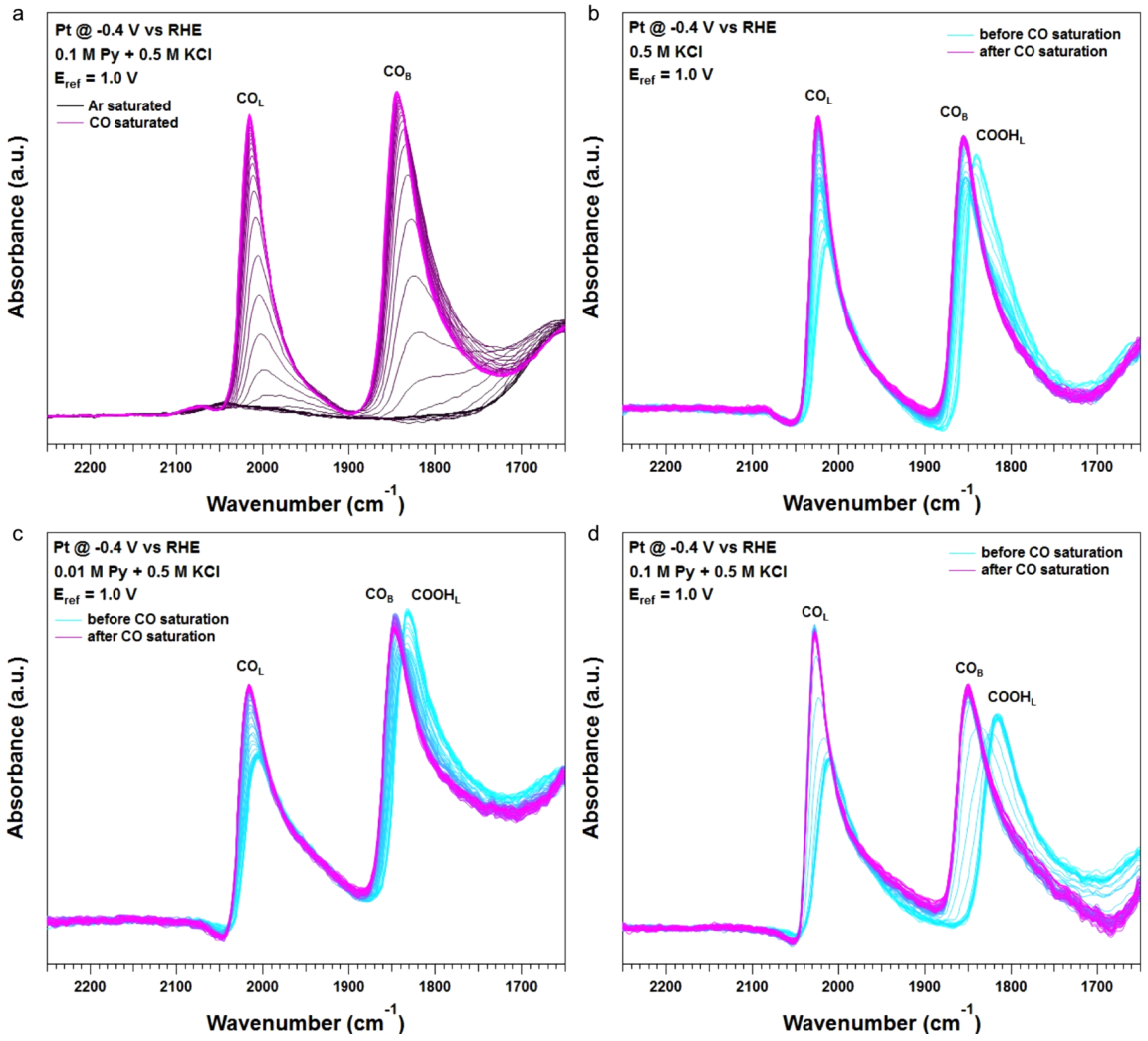

Figure 2. ATR-SEIRA spectra (4 cm^{-1} resolution, eight coadded scans) during potentiostatic electrolysis at −0.4 V in (a) 0.1 M Py and 0.5 M KCl under 1 atm CO on a Pt film electrode after Ar saturation. Spectra collected during CO purge from an initially CO_2 saturated solution in (b) 0.5 M KCl, (c) 0.01 M Py and 0.5 M KCl, and (d) 0.1 M Py and 0.5 M KCl on Pt-film electrodes. The pH of each solution was adjusted to 5.3 prior to each experiment. Reference spectra were collected at 1.0 V prior to the addition of CO.

(Figure 2b) indicates that there is more than one species contributing to this band, and the initial dip in intensity corresponds to the displacement of one species by another. We propose that the lower wavenumber band corresponds to a convolution of CO_B and $COOH_L$, and the initial decrease in intensity of the lower wavenumber band is due primarily to displacement of $COOH_L$ by the adsorbed CO (either CO_L or CO_B, Figure 3b). This assignment is also consistent with the more dramatic blue shift of the lower wavenumber band from Figure 1 to Figure 2b (1784 cm^{-1} at −0.4 V in Figure 1 to 1840 cm^{-1} in the initial CO_2-saturated spectrum of Figure 2b), which is likely due to an increase in CO_B coverage with time relative to the lower wavenumber $COOH_L$. During the initial growth of the lower wavenumber band in Figure 2d under CO_2 (Figure S7 in the Supporting Information), the band emerges at 1740 cm^{-1} and slowly shifts to 1815 cm^{-1} as the surface fraction of CO_B increases and comprises a larger portion of the lower band. Note that the unconvoluted CO_B band appears initially above 1800 cm^{-1} (Figure 2a). The dramatic difference in peak position is strong evidence that the lower wavenumber band is a convolution of both CO_B and $COOH_L$. Although deconvolution of the peak is difficult due to the shifts of peak position with both composition and coverage of surface species, the $COOH_L$ band is likely centered around 1750−1780 cm^{-1} on the basis of both the initial position of the band (Figure 1 and Figure S7) and accepted peak positions of analogous bands of similar species such as the $\nu_{C=O}$ band of aqueous formic acid (~1760 cm^{-1}) and the $\nu_{C=O}$ band of unidentate methoxycarbonyl species (~1650 cm^{-1}) on Au(111).[31,32] We emphasize that the proposed $COOH_L$ species is structurally different from adsorbed formate, which binds in a bidentate or bridge configuration via both oxygen atoms and exhibits a band at ~1320 cm^{-1} assigned to the symmetric ν_{OCO}[33] and is not observed in this study. As the CO purge continues, the coverage of CO_B increases and the lower wavenumber peak once again begins to increase.

The same qualitative behavior was observed when the previous experiment was repeated in solutions with 0.01 and 0.1 M Py (Figure 3c–f). The growth of two peaks near 2010 and 1830 cm^{-1} was observed during electrolysis under CO_2 at −0.4 V. When the purge gas was switched from CO_2 to CO, the CO_L peak near 2010 cm^{-1} grew monotonically, while the intensity of the 1830 cm^{-1} band attributed to a combination of CO_B and $COOH_L$ dipped initially followed by recovery until

DOI: 10.1021/acscatal.7b01392
ACS Catal. 2017, 7, 5410−5419

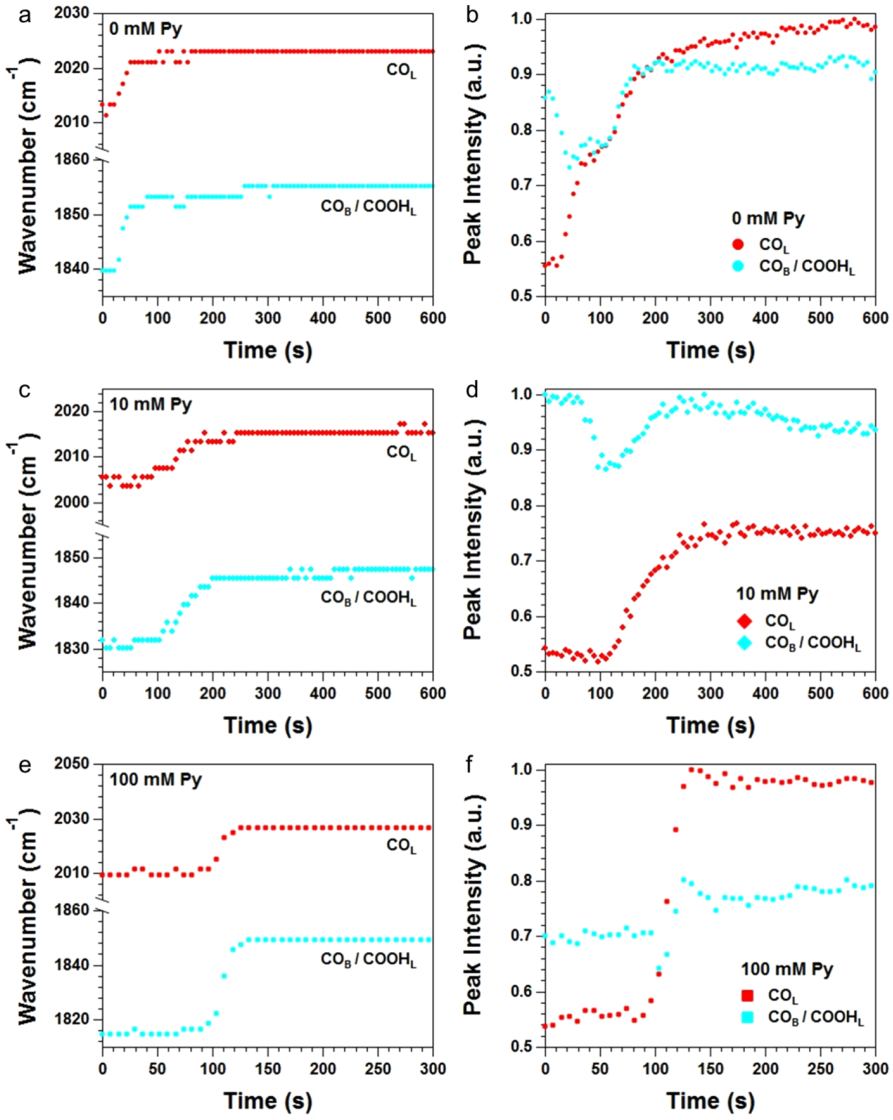

Figure 3. CO_L (red) and CO_B/$COOH_L$ (blue) peak position (a, c, e) and intensity (b, d, f) as a function of time during CO purge from an initially CO_2 saturated solution in (a, b) 0.5 M KCl, (c, d) 0.01 M Py and 0.5 M KCl, and (e, f) 0.1 M Py and 0.5 M KCl on Pt-film electrodes. The pH of each solution was adjusted to 5.3 prior to each experiment. Full spectra are given in Figure 2.

the surface reached an equilibrium coverage of CO_B. Additional evidence for the assignment of the lower wavenumber band can be found through a careful analysis of the position of this band before and after CO saturation (Figure 3a,c,e). In the absence of Py in the electrolyte, where formate selectivity relative to CO is lowest, one would expect the lowest steady-state coverage of $COOH_L$ during electrolysis and therefore the smallest contribution of $COOH_L$ to the 1830 cm^{-1} peak. Indeed, when [Py] = 0.0 M, this peak shifts only 15 cm^{-1} between the steady-state spectra under CO_2 and under CO (Figure 4, red). When [Py] = 0.01 M, the peak shift increases to 17 cm^{-1}, and at [Py] = 0.1 M, the shift grows to 35 cm^{-1}. A larger shift in peak position after CO saturation suggests that the initial peak had a larger contribution from the lower wavenumber $COOH_L$ adsorbate, corresponding to a higher relative surface coverage of $COOH_L$ to CO_B. The spectroscopic observations are consistent with the reactivity data (Figure 4, black). Adhering closely to the trend in peak shifts, the ratios of the rate of formate production to the rate of CO production are 2.6, 4.4, and 48 for 0.0, 0.01, and 0.1 M Py solutions, respectively. These

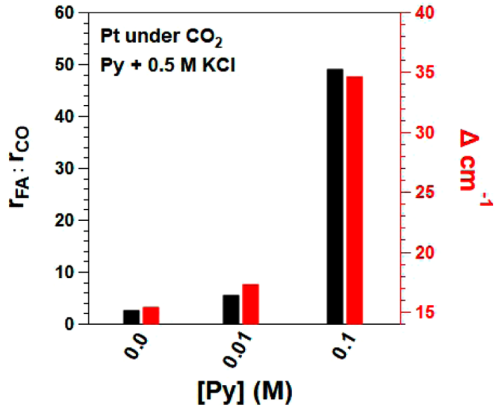

Figure 4. Ratio of the rate of formic acid to CO production during electrolysis experiments summarized in Table 2 with 0.0, 0.01, and 0.1 M Py (left axis, black) and the shift in the lower wavenumber band position upon CO saturation as shown in Figure 2b–d (right axis, red).

DOI: 10.1021/acscatal.7b01392
ACS Catal. 2017, 7, 5410–5419

correlations, along with the nonmonotonic growth of the lower wavenumber peak, are strong evidence that the peak is a convolution of the CO (CO_B and CO_L) and formate ($COOH_L$) intermediates. It is important to note that the observation of a surface-bound intermediate ($COOH_L$) is not predicted on the basis of the latest mechanistic proposals by Bocarsly et al., in which it is suggested that formate is formed through the reaction of a PyH^+-CO_2 complex with H_{ad}.[17,18] The appearance of $COOH_L$ suggests that formate is formed directly on the electrode, with its intermediate bound to the Pt electrode through a Pt−C bond, rather than in solution through interaction with a previously formed H_{ad}.

We now shift our attention to the behavior of both Py and PyH^+ as a function of potential to understand the role of Py in the CO_2RR. To study their interactions with the surface as a function of potential, independent of any interaction with CO_2, the cathode potential was stepped from 1.0 to −0.4 V, collecting spectra every 0.1 V in a solution of 0.1 M Py and 0.5 M KCl at pH 5.3 under an Ar purge (Figure 5). Above 0.7 V,

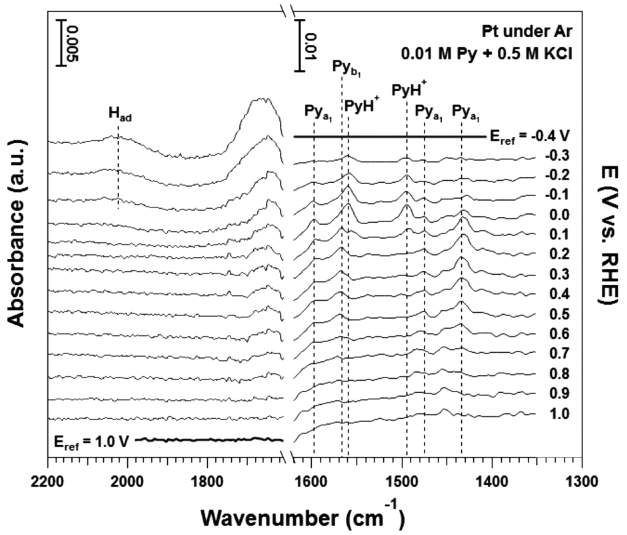

Figure 5. ATR-SEIRA spectra (4 cm^{-1} resolution, 64 coadded scans) during potentiostatic electrolysis from 1.0 to −0.4 V in 0.01 M Py and 0.5 M KCl under 1 atm of Ar on a Pt-film electrode. The pH was adjusted to 5.3 prior to spectroscopic experiments. The reference spectra for the left and right halves are set to 1.0 and −0.4 V, respectively, for clarity.

both Py (1599, 1568, 1475, and 1435 cm^{-1}) and PyH^+ (1560, 1495 cm^{-1}) peaks are minimized due to the increase in anion (primarily Cl^-) concentration near the electrode and the repulsion of PyH^+ cations by the positively charged electrode (Scheme 1a). As the potential is decreased to below 0.7 V, each of the Py peaks increase due to a decrease in Cl^- concentration near the less positively charged electrode (Scheme 1b). Additionally, both PyH^+ peaks (1560 and 1495 cm^{-1}), assigned to in-plane stretching modes of PyH^+, exhibit a significant increase beginning at 0.1 V, reaching a maximum at 0.0 V.[34] As the electrode potential is decreased below 0.0 V, the Py peaks decrease, likely due to displacement by cations (primarily K^+) in the outer Helmholtz plane, analogous to the displacement by Cl^- above 0.7 V (Scheme 1c).[19] The PyH^+ peaks also begin to decrease below −0.1 V as the current density begins to climb during potential cycling under the same conditions (Figure S2 in the Supporting Information). This increase in current is

Scheme 1. Schematic Representation of the Proposed Relative Concentrations of Each Species near the Electrode (a) from 1.0 to 0.7 V, (b) from 0.6 to −0.1 V, and (c) from −0.1 to −0.4 V during the Py-CO_2RR

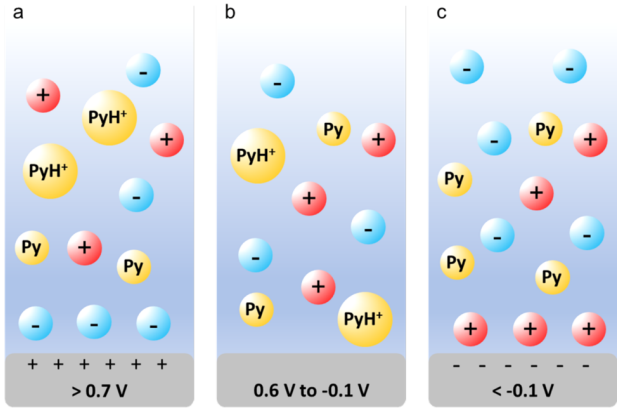

accompanied by an increase in pH near the electrode surface, which shifts the equilibrium between Py and PyH^+ back to Py, causing a decrease in [PyH^+] in the region sampled by SEIRAS (within 5−10 nm of the electrode[35]). By comparing the spectra in Figure 5 with CVs collected under the same conditions (Figure S2), we find that the maximum of the PyH^+ peaks is concurrent with the cathodic reduction peak assigned to the reduction of PyH^+ to Py and H_{ad} in the CV. This correlation suggests that the PyH^+ peaks observed in the spectra are PyH^+ ions orienting perpendicular to the Pt surface in an H-down configuration prior to reduction at the Pt-film electrode according to the surface selection rules for ATR-SEIRAS, which state that only vibrational modes with dipole changes perpendicular to the surface are SEIRAS active.[35]

Potential-dependent spectra of the Py-CO_2RR on Pt collected in 0.01 M Py and 0.5 M KCl under a CO_2 purge exhibit Py and PyH^+ similar to those observed under Ar (Figure 6), with a few key differences. In contrast to the Ar-saturated system, the 1568 and 1425 cm^{-1} bands, assigned to the a_1 ring deformation mode of Py (with a dipole change along the C_2 axis of Py, Figure 6 inset), and the b_1 ring deformation mode of Py (with a dipole change perpendicular to the C_2 axis of Py), respectively, show a significant signal at 1.0 V.[36] Since there is no preferred orientation of Py in the bulk phase, the simultaneous increase and decrease of a_1 and b_1 modes entails the increase and decrease of the concentration of dissolved Py at the electrochemical interface, respectively. Thus, the increase in both the a_1 and b_1 bands of Py at high potentials in the presence of CO_2 relative to Ar suggests that the acid−base interactions between Py and CO_2 in solution increases CO_2 concentration near the electrode, which contributes to, if not accounts for, the increased activity in the presence of Py. It is important to note that the solubility of CO_2 increases from 34 to 55 mM in the presence of 0.01 M Py at pH 5.3 on the basis of solution equilibria (Table S2 in the Supporting Information). The appearance of both a_1 and b_1 bands in conjunction, as well as the insensitivity of peak position to electrode potential (lack of the Stark tuning effect), suggests that the Py bands observed above 0.1 V are due to Py in the electrolyte near the electrode, rather than directly adsorbed on the Pt surface: i.e., there is no preferential orientation of near-electrode Py, as dictated by the surface selection rules for ATR-SEIRAS. Unlike the Py bands, the PyH^+ bands show behavior nearly identical with those in

DOI: 10.1021/acscatal.7b01392
ACS Catal. 2017, 7, 5410−5419

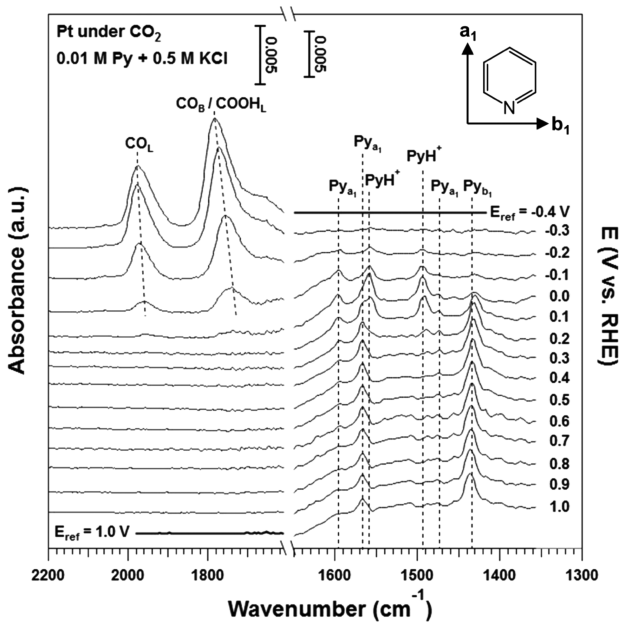

Figure 6. ATR-SEIRA spectra (4 cm^{-1} resolution, 64 coadded scans) during potentiostatic electrolysis from 1.0 to −0.4 V in 0.01 M Py and 0.5 M KCl under 1 atm of CO_2 on a Pt-film electrode. The pH was adjusted to 5.3 prior to CO_2 saturation with H_2SO_4 and does not change upon addition of CO_2. Reference spectra for the left and right halves are set to 1.0 and −0.4 V, respectively, for clarity. Inset: schematic representation of the direction of dipole changes corresponding to the a_1 and b_1 bands of Py.

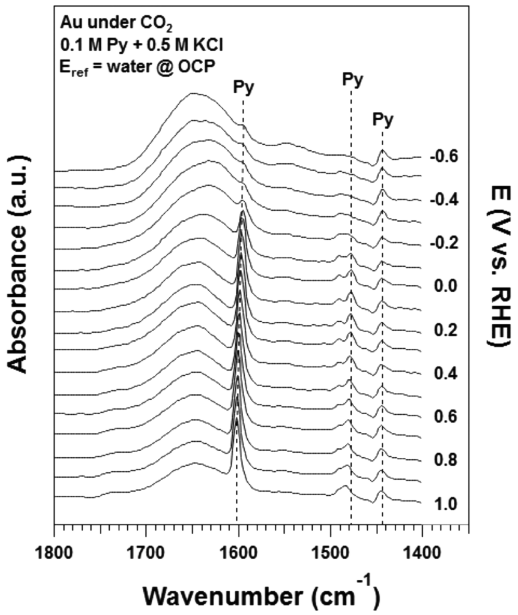

Figure 7. ATR-SEIRA spectra (4 cm^{-1} resolution, 64 coadded scans) during potentiostatic electrolysis from 1.0 to −0.6 V in 0.1 M Py and 0.5 M KCl under 1 atm of CO_2 on an Au-film electrode. The pH was adjusted to 5.3 prior to CO_2 saturation with H_2SO_4 and does not change upon addition of CO_2. The reference spectrum was collected in distilled water at open circuit potential prior to the addition of Py or the supporting electrolyte.

the Ar-saturated system. Moreover, the growth of CO_L and $CO_B/COOH_L$ peaks with decreasing potential (below 0.0 V) show the same qualitative behavior as the spectra in the absence of Py (Figure 1), with one key difference. The onset potential of the CO_L and $CO_B/COOH_L$ bands is earlier (higher potential) in the absence of Py. This result is somewhat unexpected considering the higher reaction rates observed in the presence of Py. A possible explanation for the delayed onset of the CO_2RR in the presence of Py is that the formation of the Py−CO_2 pair leads to a larger overpotential in the initial formation of the $COOH_L$ intermediate due to the loss of the favorable Py−CO_2 interaction. Together these observations suggest that there is no drastic mechanistic change in the CO_2RR caused by the addition of Py beyond the additional route to hydrogen adsorption through the reduction of the PyH^+ cation and the increased CO_2 solubility though Py−CO_2 interactions (Table S2). The effect of increasing Py concentration was also tested by conducting an analogous experiment with 0.1 M Py (Figure S8 in the Supporting Information), which shows the same qualitative behavior as the 0.01 M Py case, with larger Py and PyH^+ peaks due to the overall concentration increase in the 0.1 M Py solution. This indicates that the general structure of the electrode−electrolyte interface, as well as the reaction mechanism, is independent of the Py concentration.

Py-CO_2RR on Au Electrodes. Previous studies using cyclic voltammetry on various electrodes suggest that the reduction of PyH^+ to Py and H_{ad} on Pt or Pd electrodes is the key to the promotion of the electrochemical reduction of CO_2 on these typically CO_2RR-inactive metals.[7,15−18,37] This hypothesis was tested by collecting SEIRA spectra on an Au-film electrode in 0.1 M Py and 0.5 M KCl at pH 5.3 under a CO_2 purge (Figure 7). In sharp contrast to Pt, no adsorbed CO was observed, which is due to the displacement of the adsorbed CO intermediate at low potentials by cations.[19,23] Additionally, no $COOH_L$ intermediate was observed within the potential range tested. This finding is in good agreement with corresponding electrolysis results that showed no formate was produced on Au-foil electrodes.[37,38] Furthermore, no change in bands corresponding to PyH^+ were observed during electrolysis with the Au-film electrode across the entire potential range tested. The lack of change in PyH^+ bands with potential is additional evidence supporting our previous assertion that the two peaks at ∼1560 and 1495 cm^{-1} observed on Pt-film electrodes around 0.0 V are due not simply to bulk PyH^+ but to PyH^+ preferentially oriented perpendicular to the electrode surface prior to reduction to Py and H_{ad}. In contrast with their behavior on Pt, the intensity of the band corresponding to the a_1 mode of Py reaches a maximum intensity at 1.0 V on Au and decreases monotonically with decreasing potential. The observed decrease in a_1 Py bands on Au is in good agreement with previous spectroscopic investigations of Py adsorption on Au, which suggest that at higher potential Py is oriented perpendicular to the Au electrode with the nitrogen facing the Au surface, while as the potential is decreased, the near-surface Py tends to tilt, causing a decrease in the a_1 ring deformation bands.[36] The observed tilting of near-surface Py could be due to increase in cation concentration near the cathode with decreasing potential.[19] The b_1 band is independent of potential, suggesting that the small peak observed at 1444 cm^{-1} is due to Py in the bulk solution, rather than at the electrode surface. It may be expected, as proposed on Pt electrodes, that Cl^- anions drawn to the Au surface at 1.0 V would cause a minimum in Py bands. The seeming disparity can be explained by the weaker interaction between Au and Cl^- relative to Pt, where Cl^- has

DOI: 10.1021/acscatal.7b01392
ACS Catal. 2017, 7, 5410−5419

Scheme 2. Proposed Reaction Mechanism of the Py-CO_2RR on Pt Electrodes on the Basis of Both Reactivity and Spectroscopic Data

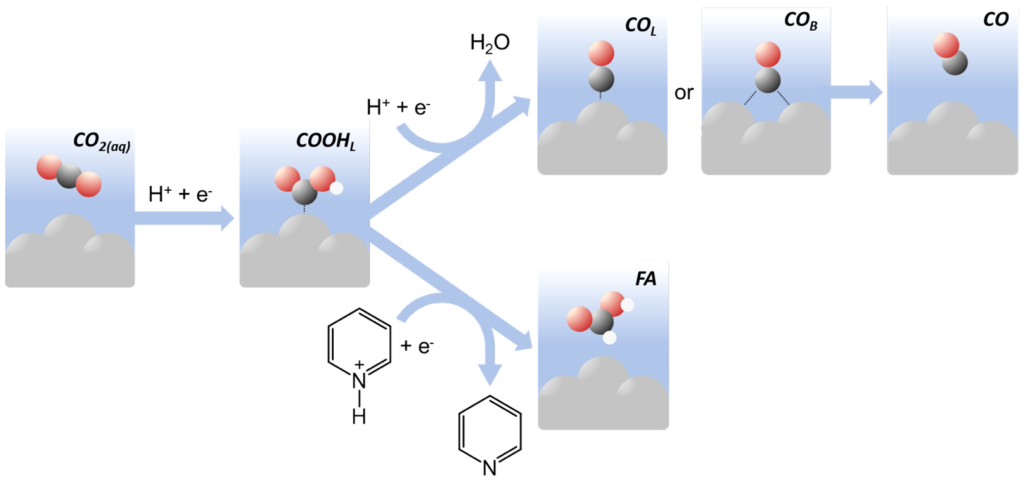

been shown to be a significant poison at sufficiently high electrode potentials.[39]

On the basis of both electrochemical reactivity and spectroscopic results, we propose that the presence of Py promotes the CO_2RR through an increased CO_2 concentration in the electrolyte due to the favorable acid−base interaction between Py and dissolved CO_2 in solution. Additionally, the direct observation of the $COOH_L$ intermediate suggests that the Py-CO_2RR to both CO and formate proceeds through an initial proton-coupled electron transfer step, wherein $COOH_L$ is formed directly on the electrode, as proposed in previous studies of the CO_2RR to CO on Au, Ag, and Pd electrodes (Scheme 2).[40−42] It is important to note that this observation is in contrast to previous mechanistic proposals of the Py-CO_2RR which suggest that formate is produced not through a surface-bound carbonaceous intermediate but through the reaction of the Py−CO_2 complex with H_{ad}.[18] Neither this work nor previous spectroscopic studies of the CO_2RR on Au electrodes observed the $COOH_L$ intermediate, likely due to a lower residence time or surface coverage on Au.[23,43] On the basis of both reactivity studies, which show enhanced formic acid selectivity and production rates in the presence versus the absence of Py (Tables 1 and 2), and spectroscopic studies, which show that the relative surface coverage of $COOH_L$ to CO_B increases with increasing Py concentration (Figures 2 and 3), we suggest that the presence of Py during the CO_2RR promotes the formation of formate through the selective protonation of the C (rather than the OH to form CO_{ad}) of the $COOH_L$ intermediate by PyH^+. Additionally, the reaction rate is likely improved by the increased solubility and potentially improved transport of CO_2 to the electrode surface. The reaction rate may also be improved by the ability of PyH^+ to act as a proton donor in the initial proton-coupled electron transfer step in which the $COOH_L$ intermediate is produced. The increased selectivity toward formate rather than CO at higher Py concentrations is proposed to be due to the preferential donation of the PyH^+ to the C of the $COOH_L$ intermediate rather than the hydroxyl group as in the CO production pathway.

CONCLUSIONS

Careful reactivity studies of the Py-CO_2RR were unable to replicate previous claims of methanol production on Pt electrodes; however, reactivity studies suggest that the addition of Py to the electrolyte promotes the formation of formate over both H_2 and CO through the selective protonation of the C over the hydroxyl group of the $COOH_L$ intermediate. In situ ATR-SEIRAS studies support the previous assignment of the cathodic peak during CV to the reduction of PyH^+ to Py. Importantly, the observation of the surface-bound $COOH_L$ intermediate suggests that formate is produced directly on the electrode, rather than through the reaction of a Py−CO_2 complex with H_{ad}. The decrease in PyH^+ bands suggests that the rate of the Py-CO_2RR is potentially limited by the decrease of near-surface PyH^+ due to an increase in surface pH as the rate of the HER increases. Finally, we show that the reduction of PyH^+ to H_{ad} and Py does not occur on Au electrodes in the potential range studied (1.0 to −0.6 V), consistent with the conclusions of Lebègue et al.

ASSOCIATED CONTENT

Supporting Information

The Supporting Information is available free of charge on the ACS Publications website at DOI: 10.1021/acscatal.7b01392.

Electrochemical cell schematics, cyclic voltammograms, spectra, and reactivity studies (PDF)

AUTHOR INFORMATION

Corresponding Authors

*E-mail for Y.Y.: yanys@udel.edu.
*E-mail for B.X.: bxu@udel.edu.

ORCID

Bingjun Xu: 0000-0002-2303-257X

Author Contributions

Experiments were performed by M.D. The manuscript was written through contributions of all authors, and all authors have given approval to the final version of the manuscript.

Notes

The authors declare no competing financial interest.

ACKNOWLEDGMENTS

B.X. acknowledges the support of the National Science Foundation CAREER Program (Award No. CBET-1437129). M.D. and Y.Y. acknowledge the support of the National Science

DOI: 10.1021/acscatal.7b01392
ACS Catal. 2017, 7, 5410−5419

Foundation-Chemical Catalysis Program (Award No. CHE-1566138).

REFERENCES

(1) Gattrell, M.; Gupta, N.; Co, A. *J. Electroanal. Chem.* **2006**, *594*, 1−19.
(2) Hori, Y. In *Modern Aspects of Electrochemistry*; Vayenas, C., White, R., Gamboa-Aldeco, M., Eds.; Springer: New York, 2008; Vol. *42*, pp 89−189.
(3) Lu, Q.; Rosen, J.; Jiao, F. *ChemCatChem* **2015**, *7*, 38−47.
(4) Hori, Y.; Wakebe, H.; Tsukamoto, T.; Koga, O. *Electrochim. Acta* **1994**, *39*, 1833−1839.
(5) Seshadri, G.; Lin, C.; Bocarsly, A. B. *J. Electroanal. Chem.* **1994**, *372*, 145−150.
(6) Costentin, C.; Canales, J. C.; Haddou, B.; Savéant, J.-M. *J. Am. Chem. Soc.* **2013**, *135*, 17671−17674.
(7) Portenkirchner, E.; Enengl, C.; Enengl, S.; Hinterberger, G.; Schlager, S.; Apaydin, D.; Neugebauer, H.; Knör, G.; Sariciftci, N. S. *ChemElectroChem* **2014**, *1*, 1543−1548.
(8) Barton Cole, E.; Lakkaraju, P. S.; Rampulla, D. M.; Morris, A. J.; Abelev, E.; Bocarsly, A. B. *J. Am. Chem. Soc.* **2010**, *132*, 11539−11551.
(9) Morris, A. J.; McGibbon, R. T.; Bocarsly, A. B. *ChemSusChem* **2011**, *4*, 191−196.
(10) Keith, J. A.; Carter, E. A. *J. Am. Chem. Soc.* **2012**, *134*, 7580−7583.
(11) Keith, J. A.; Carter, E. A. *J. Phys. Chem. Lett.* **2013**, *4*, 4058−4063.
(12) Keith, J. A.; Carter, E. A. *Chem. Sci.* **2013**, *4*, 1490−1496.
(13) Lim, C.-H.; Holder, A. M.; Hynes, J. T.; Musgrave, C. B. *J. Am. Chem. Soc.* **2014**, *136*, 16081−16095.
(14) Lim, C.-H.; Holder, A. M.; Musgrave, C. B. *J. Am. Chem. Soc.* **2013**, *135*, 142−154.
(15) Ertem, M. Z.; Konezny, S. J.; Araujo, C. M.; Batista, V. S. *J. Phys. Chem. Lett.* **2013**, *4*, 745−748.
(16) Yan, Y.; Zeitler, E. L.; Gu, J.; Hu, Y.; Bocarsly, A. B. *J. Am. Chem. Soc.* **2013**, *135*, 14020−14023.
(17) Barton Cole, E. E.; Baruch, M. F.; L'Esperance, R. P.; Kelly, M. T.; Lakkaraju, P. S.; Zeitler, E. L.; Bocarsly, A. B. *Top. Catal.* **2015**, *58*, 15−22.
(18) Zeitler, E. L.; Ertem, M. Z.; Pander, J. E.; Yan, Y.; Batista, V. S.; Bocarsly, A. B. *J. Electrochem. Soc.* **2015**, *162*, H938−H944.
(19) Dunwell, M.; Wang, J.; Yan, Y.; Xu, B. *Phys. Chem. Chem. Phys.* **2017**, *19*, 971−975.
(20) Dunwell, M.; Yan, Y.; Xu, B. *Surf. Sci.* **2016**, *650*, 51−56.
(21) Falbe-Hansen, H.; Sørensen, S.; Jensen, N. R.; Pedersen, T.; Hjorth, J. *Atmos. Environ.* **2000**, *34*, 1543−1551.
(22) Vandresen, S.; Resende, S. M. *J. Phys. Chem. A* **2004**, *108*, 2284−2289.
(23) Dunwell, M.; Lu, Q.; Heyes, J. M.; Rosen, J.; Chen, J. G.; Yan, Y.; Jiao, F.; Xu, B. *J. Am. Chem. Soc.* **2017**, *139*, 3774−3783.
(24) Lambert, D. K. *Solid State Commun.* **1984**, *51*, 297−300.
(25) Lambert, D. K. *Electrochim. Acta* **1996**, *41*, 623−630.
(26) Kunimatsu, K.; Senzaki, T.; Samjeské, G.; Tsushima, M.; Osawa, M. *Electrochim. Acta* **2007**, *52*, 5715−5724.
(27) Kunimatsu, K.; Senzaki, T.; Tsushima, M.; Osawa, M. *Chem. Phys. Lett.* **2005**, *401*, 451−454.
(28) Kunimatsu, K.; Uchida, H.; Osawa, M.; Watanabe, M. *J. Electroanal. Chem.* **2006**, *587*, 299−307.
(29) Kunimatsu, K.; Sato, T.; Uchida, H.; Watanabe, M. *Langmuir* **2008**, *24*, 3590−3601.
(30) Yan-Gang; Li, Q.-X.; Huo, S.-J.; Ma, M.; Cai, W.-B.; Osawa, M. *J. Phys. Chem. B* **2005**, *109*, 7900−7906.
(31) Cuesta, A.; Cabello, G.; Osawa, M.; Gutiérrez, C. *ACS Catal.* **2012**, *2*, 728−738.
(32) Xu, B.; Madix, R. J.; Friend, C. M. *J. Am. Chem. Soc.* **2011**, *133*, 20378−20383.
(33) Miki, A.; Ye, S.; Senzaki, T.; Osawa, M. *J. Electroanal. Chem.* **2004**, *563*, 23−31.
(34) Castellà-Ventura, M.; Akacem, Y.; Kassab, E. *J. Phys. Chem. C* **2008**, *112*, 19045−19054.
(35) Osawa, M. In *Near-Field Optics and Surface Plasmon Polaritons*; Kawata, S., Ed.; Springer: Berlin, Heidelberg, 2001; Vol. *81*, pp 163−187.
(36) Li, N.; Zamlynny, V.; Lipkowski, J.; Henglein, F.; Pettinger, B. *J. Electroanal. Chem.* **2002**, *524*−*525*, 43−53.
(37) Lebègue, E.; Agullo, J.; Morin, M.; Bélanger, D. *ChemElectroChem* **2014**, *1*, 1013−1017.
(38) Lucio, A. J.; Shaw, S. K. *J. Phys. Chem. C* **2015**, *119*, 12523−12530.
(39) Arruda, T. M.; Shyam, B.; Ziegelbauer, J. M.; Mukerjee, S.; Ramaker, D. E. *J. Phys. Chem. C* **2008**, *112*, 18087−18097.
(40) Rosen, J.; Hutchings, G. S.; Lu, Q.; Rivera, S.; Zhou, Y.; Vlachos, D. G.; Jiao, F. *ACS Catal.* **2015**, *5*, 4293−4299.
(41) Sheng, W.; Kattel, S.; Yao, S.; Yan, B.; Liang, Z.; Hawxhurst, C.; Wu, Q.; Chen, J. G. *Energy Environ. Sci.* **2017**, *10*, 1180−1185.
(42) Zhu, W.; Michalsky, R.; Metin, Ö.; Lv, H.; Guo, S.; Wright, C. J.; Sun, X.; Peterson, A. A.; Sun, S. *J. Am. Chem. Soc.* **2013**, *135*, 16833−16836.
(43) Wuttig, A.; Yaguchi, M.; Motobayashi, K.; Osawa, M.; Surendranath, Y. *Proc. Natl. Acad. Sci. U. S. A.* **2016**, *113*, E4585−E4593.

DOI: 10.1021/acscatal.7b01392
ACS Catal. 2017, 7, 5410−5419